Bandgap energy bowing parameter of strained and relaxed InGaN layers,

Gaëlle Orsal, Youssef El Gmili, Nicolas Fressengeas, Jérémy Streque, Ryad Djerboub, Tarik Moudakir, Sundaram Suresh, Abdallah Ougazzaden, Jean-Paul Salvestrini

Bandgap energy bowing parameter of strained and relaxed InGaN layers

G. Orsal,[1,2,3,*] **Y. El Gmili,**[3] **N. Fressengeas,**[1,2,3] **J. Streque,**[3]
R. Djerboub,[1,2,3] **T. Moudakir,**[3] **S. Sundaram,**[3]
A. Ougazzaden,[3,4] **and J.P. Salvestrini**[1,2,3]

[1]*Université de Lorraine, LMOPS, EA 4423, 2 rue E. Belin, 57070 Metz, France*
[2]*Supélec, LMOPS, EA 4423, 2 rue E. Belin, 57070 Metz, France*
[3]*CNRS UMI GT-CNRS 2958, 2-3 rue Marconi, 57070, Metz, France*
[4]*Georgia Institute of Technology, UMI GT-CNRS 2958, 2-3 rue Marconi, 57070, Metz, France*
[*]*gaelle.orsal@metz.supelec.fr*

Abstract: This paper focuses on the determination of the bandgap energy bowing parameter of strained and relaxed $In_xGa_{1-x}N$ layers. Samples are grown by metal organic vapor phase epitaxy on GaN template substrate for indium compositions in the range of $0<x<0.25$. The bangap emission energy is characterized by cathodoluminescence and the indium composition as well as the strain state are deduced from high resolution X-ray diffraction measurements. The experimental variation of the bangap emission energy with indium content can be described by the standard quadratic equation, fitted using a relative least square method and qualified with a chi square test. Our approach leads to values of the bandgap energy bowing parameter equal to 2.87±0.20eV and 1.32±0.28eV for relaxed and strained layers (determined for the first time since the revision of the InN bandgap energy in 2002), respectively. The corresponding modified Vegard's laws describe accurately the indium content dependence of the bandgap emission energy in InGaN alloy and for the whole range of indium content. Finally, as an example of application, 3D mapping of indium content in a thick InGaN layer is deduced from bandgap energy measurements using cathodoluminescence and a corresponding hyperspectral map.

© 2014 Optical Society of America

OCIS codes: (310.6860) Thin films, optical properties; (120.0120) Instrumentation, measurement and metrology.

References and links

1. J. Zhang, and N. Tansu, "Improvement in spontaneous emission rates for InGaN quantum wells on ternary InGaN substrate for light-emitting diodes," J. Appl. Phys. **110,** 113110-1–113110-5 (2011).
2. P. S. Hsu, M. T. Hardy, F. Wu, I. Koslow, E. C. Young, A. E. Romanov, K. Fujito, D. F. Feezell, S. P. DenBaars, J. S. Speck, and S. Nakamura, "444.9nm semipolar (1122) laser diode grown on an intentionally stress relaxed InGaN waveguiding layer," Appl. Phys. Lett. **100,** 021104-1–021104-4 (2012).
3. J. Zhang, and N. Tansu, "Optical Gain and Laser Characteristics of InGaN Quantum Wells on Ternary InGaN Substrates," IEEE Photon. J. **5,** 2600111 (2013).
4. C. J. Neufeld, N. G. Toledo, S. C. Cruz, M. Iza, S. P. DenBaars, and U. K. Mishra, "High quantum efficiency InGaN/GaN solar cells with 2.95 eV bandgap," Appl. Phys. Lett. **93,** 143502-1–143502-3 (2008).
5. E. Matioli, C. Neufeld, M. Iza, S. C. Cruz, A. A. Al-Heji, X. Chen, R. M. Farrell, S. Keller, S. DenBaars, U. Mishra, S. Nakamura, J. Speck, and C. Weisbuch, "High internal and external quantum efficiency InGaN/GaN solar cells," Appl. Phys. Lett. **98,** 021102-1–021102-3 (2011).

6. J. R. Lang, C. J. Neufeld, C. A. Hurni, S. C. Cruz, E. Matioli, U. K. Mishra, and J. S. Speck, "High external quantum efficiency and fill-factor InGaN/GaN heterojunction solar cells grown by NH_3-based molecular beam epitaxy," Appl. Phys. Lett. **98,** 131115-1–131115-3 (2011).

7. X. Cai, S. Zeng, and B. Zhang, "Fabrication and characterization of InGaN p-i-n homojunction solar cell," Appl. Phys. Lett. **95,** 173504-1–173504-3 (2009).

8. M. R. Islam, M. R. Kaysir, M. J. Islam, A. Hashimoto, and A. Yamamoto, "MOVPE Growth of $In_xGa_{1-x}N$ (x $\approx$ 0.4) and Fabrication of Homo-junction Solar Cells," J. Mater. Sci. Technol., **29**(2), 128-136 (2013).

9. M. Moret, B. Gil, S. Ruffenach, O. Briot, Ch. Giesen, M. Heuken, S. Rushworth, T. Leese, and M. Succi, "Optical, structural investigations and band-gap bowing parameter of GaInN alloys," J. Cryst. Growth **311,** 2795-2797 (2009).

10. M. Kurouchi, T. Araki, H. Naoi, T. Yamaguchi, A. Suzuki, and Y. Nanish, "Growth and properties of In-rich InGaN films grown on (0001) sapphire by RF-MBE," Phys. Stat. Sol. (B), **241,** 2843-2848 (2004).

11. J. Wu, W. Walukiewicz, K. M. Yu, J. W. Ager, E. E. Haller, H. Lu, and W. J. Schaff, "Small bandgap bowing in $In_{1-x}Ga_xN$ alloys," Appl. Phys. Lett., **80,** 4741-4743 (2002).

12. C. A. Parker, J. C. Roberts, S. M. Bedair, M. J. Reed, S. X. Liu, and N. A. El- Masry, "Determination of the critical layer thickness in the InGaN/GaN Heterostructures," Appl. Phys. Lett., **75**(18), 2776-2778 (1999).

13. P. A. Ponce, S. Srinivasan, A. Bell, L. Geng, R. Liu, M. Stevens, J. Cai, H. Omiya, H. Marui, and S. Tanaka, "Microstructure and electronic properties of InGaN alloys," Phys. Stat. Sol. B **240,** 273-284 (2003).

14. W. Shan, W. Walukiewicz, E. E. Haller, B. D. Little, J. J. Song, M. D. McCluskey, N. M. Johnson, Z. C. Feng, M. Schurman and R. A. Stall, "Optical properties of $In_xGa_{1-x}N$ alloys grown by metalorganic chemical vapor deposition," J. Appl. Phys., **84,** 4452-4458 (1998).

15. Z. C. Feng, W. Liu, S. J. Chua, J. W. Yu, C. C. Yang, T. R. Yang, and J. Zhao, "Photoluminescence characteristics of low indium composition InGaN thin films grown on sapphire by metalorganic chemical vapor deposition," Thin Sol. Films **498,** 118-122 (2006).

16. F. B. Naranjo, S. Fernanchez-Garcia, F. Calle, E. Calleja, A. Trampert, and KH. Ploog, "Structural and optical characterization of thick InGaN layers and InGaN/GaN MQW grown by molecular beam epitaxy," Mater. Sci. Eng. B, **93,** 131-134 (2002).

17. J-P. Nougier, *Méthode des calculs numériques. Volume 2, Fonctions équations aux dérivées* (Hermes Science Publications, 2001).

18. S. Gautier, C. Sartel, S. Ould-Saad, J. Martin, A. Sirenko, and A. Ougazzaden, "GaN materials growth by MOVPE in a new-design reactor using DMHy and NH_3," J. Cryst. Growth **298,** 428-432 (2007).

19. M. A. Moram, and M. E. Vickers, "X-ray diffraction of III-nitrides," Rep. Prog. Phys., **72,** 036502-1– 036502-40 (2009).

20. M. Schuster, P. O. Gervais, B. Jobst, W. H. Osler, R. Averbeck, H. Riechert, A. Iberlk, and R. Stmmerk, "Determination of the chemical composition of distorted InGaN/GaN heterostructures from x-ray diffraction data," J. Phys. D: Appl. Phys. **32**, A56-A60 (1999).

21. Y. El Gmili, G. Orsal, K. Pantzas, A. Ahaitouf, T. Moudakir, S. Gautier, G. Patriarche, D. Troadec, J. P. Salvestrini, and A. Ougazzaden, "Characteristics of the surface microstructures in thick InGaN layers on GaN," Opt. Mat. Exp. **3**(8), 1111-1118 (2013).

22. Y. El Gmili, G. Orsal, K. Pantzas, T. Moudakir, S. Sundaram, G. Patriarche, J. Hester, A. Ahaitouf, J. P. Salvestrini and A. Ougazzaden, "Multilayered InGaN/GaN structure vs. single InGaN layer for solar cell applications: A comparative study," Act. Mat. **61**(17), 6587-6596 (2013).

23. A. Fischer, H. Kuhne, and H. Richter, "New Approach in Equilibrium Theory for Strained Layer Relaxation," Phys. Rev. Lett., **73,** 2712-2715 (1994).

24. M. Leyer, J. Stellmach, Ch. Meissner, M. Pristovsek, and M. Kneissl, "The critical thickness of InGaN on (0001) GaN," J. Cryst. Growth, **310,** 4913-4915 (2008).

25. S. Pereira, M. R. Correia, E. Pereira, C. Trager-Cowan, F. Sweeney, K. P. ODonnell, E. Alves, N. Franco, and A. D. Sequeira, "Structural and optical properties of InGaN/GaN layers close to the critical layer thickness," Appl. Phys. Lett. **81,** 1207-1209 (2002).

26. M. A. Reshchikov, D. Huang, F. Yun, P. Visconti, L. He, H. Morkoç, J. Jasinski, Z. Liliental-Weber, R. J. Molnar, S. S. Park, and K. Y. Lee, "Unusual luminescence lines in GaN," J. Appl. Phys., **94**(9), 5623-5632 (2003).

27. M. R. Correia, S. Pereira, E. Pereira, R. A. Sa Ferreira, J. Frandonc, E. Alvesd, I. M. Watsonf, C. Liuf, A. Morelg, and B. Gilg, "Optical studies on the red luminescence of InGaN epilayers," Superlattices and Microstructures **36,** 625-632 (2004).

28. S. Pereira, M. R. Correia, E. Pereira, K. P. O'Donnell, C. Trager-Cowan, F. Sweeney, and E. Alves, "Compositional pulling effects in $In_xGa_{1-x}N$/GaN layers: A combined depth-resolved cathodoluminescence and Rutherford backscattering/channeling study," Phys. Rev. B **64**(20), 205311-1–205311-5 (2001).

29. K Pantzas, G Patriarche, D Troadec, S Gautier, T Moudakir, S Suresh, L Largeau, O Mauguin, P L Voss and A Ougazzaden, "Nanometer-scale, quantitative composition mappings of InGaN layers from a combination of scanning transmission electron microscopy and energy dispersive x-ray spectroscopy," Nanotechnology **23,** 455707-455715 (2012).

30. K. Pantzas, G. Patriarche, G. Orsal, S. Gautier, T. Moudakir, M. Abid, V. Gorge, Z. Djebbour, P. L. Voss, and

A. Ougazzaden, "Investigation of a relaxation mechanism specific to InGaN for improved MOVPE growth of nitride solar cell materials," Phys. Stat. Sol. A **209**, 25-28 (2012).

31. F. K. Yam, and Z. Hassan, "InGaN: An overview of the growth kinetics, physical properties and emission mechanisms," Superlattices and Microstructures **43**, 1-23 (2008).
32. W. Walukiewicz, "Narrow bandgap group III-nitride alloys," Physica E **20**, 300-307 (2004).
33. T. Matsuoka, H. Okamoto, M. Nakao, H. Harima, and E. Kurimoto, "Optical bandgap energy of wurtzite InN," Appl. Phys. Lett. **81**, 1246-1248 (2002).
34. Q. Yan, P. Rinke, M. Scheffler and C. G. Van, "Strain effects in group-III nitrides: Deformation potentials for AlN, GaN, and InN," Appl. Phys. Lett **95**, 121111-1–121111-3 (2009).
35. H. Y. Peng, M. M. McCluskey, Y. M. Gupta, M. Kneissl, and N. M. Johnson, "Shock-induced band-gap shift in GaN: Anisotropy of the deformation potentials," Phys. Rev. B **71**, 115207-1–115207-5 (2005).

1. Introduction

The tunability of the fundamental bandgap of indium gallium nitride (InGaN) across the full visible range spectrum has led to the development of a variety of optoelectronic devices including blue, green, red and white light-emitting diodes [1], blue and green laser diodes [2, 3], and solar cells [4–7]. For the design and the fabrication of such optoelectronic device structures an accurate knowledge of the bandgap energy as a function of the indium content in $In_xGa_{1-x}N$ alloy for both strained and relaxed layers is required. The composition dependence (x) of the bandgap can be generally described using a modified Vegard's law including, in addition to the linear interpolation, a quadratic term depending on a bowing parameter b:

$$E_{NBE}^{InGaN} = x \times E_{NBE}^{InN} + (1-x) \times E_{NBE}^{GaN} - b \times x \times (1-x) \tag{1}$$

where E_{NBE}^{GaN} and E_{NBE}^{InN} are the values of the emission energy deduced from optical measurements. However, large discrepancies are observed in the published values of b varying in the range 1.4eV-2.8eV [8–11] since the InN bangap re-evaluation in 2002 [11]. The first reason that could explain such a broad range of values of b is linked to the strain state rate of the studied $In_xGa_{1-x}N$ layers. Indeed, as shown by Parker et al. [12] and Ponce et al [13] different dependencies of the bandgap emission energy with the indium composition are expected for $In_xGa_{1-x}N$ layers according to their strain states. It is thus necessary to know the strain states of the $In_xGa_{1-x}N$ layers and determine the value of the bowing parameter accordingly. The second issue deals with the method used to measure the bandgap energy values. Indeed, the bandgap energy deduced from either photoluminescence (PL) or cathodoluminescence (CL) measurements is Stokes shifted relative to the bandgap energy determined by techniques such as photoreflection, optical absorption or transmission, leading to an underestimation of the bandgap energy for a given indium composition [8, 11, 13, 14]. Last, special attention has to be paid to the measurement temperature since the bandgap energy is expected to vary with temperature according to the well known Varshni's equation. Furthermore, due to indium compositional fluctuation or phase separation, an "S-shape" temperature dependence of the bandgap was reported for InGaN alloy with indium content as low as 3% [15, 16]. In this paper, the bandgap energy is characterized using room-temperature CL and PL. High resolution X-ray diffraction (XRD) is used to determine the indium content as well as the strain state rate of the InGaN alloys layers. For both relaxed and strained InGaN layers, the experimental bandgap energy bowing parameters were fitted using a relative least square method from the compositional dependence of the emission bandgap, and qualified by a chi square test [17]. Finally, as an example, CL hyperspectral maps of a thick InGaN layer are plotted in terms of indium content. Results highlight the phase separation issue in such thick layers.

2. Experimental

Several In$_x$Ga$_{1-x}$N samples with a wurtzite structure and different compositions of indium (0<x<0.25) and thicknesses (10-200nm) were grown on c-axis oriented GaN/sapphire template substrates in a T-shape low-pressure metal organic vapor phase epitaxy (MOVPE) reactor [18]. The growth was performed at 800°C under a reactor pressure of 100 Torr. Nitrogen (N$_2$) was used as carrier gas and trimethylgallium (TMGa), trimethylindium (TMIn) and ammonia (NH$_3$) were employed as precursor sources for Ga, In and elemental N, respectively. The layer thicknesses were deduced from in-situ reflectometry and confirmed by (0 0.2) ω-2θ XRD measurements by applying a fitting model to the Pendellösung fringes. Symmetric (0 0.4) ω-2θ scans in combination with XRD reciprocal space maps (RSMs) of the asymmetric (1 1.4) and (1 0.5) planes were used to determine the lattice parameters (a, c) and the degree of relaxation of the InGaN layer. Depending on the strain state, the indium composition can be calculated according to the following procedure. For unstrained layers (fully relaxed films), the composition x is deduced from the well known Vegard's law:

$$x = \frac{c_{mes}^{InGaN} - c_{mes}^{GaN}}{c_0^{InN} - c_{mes}^{GaN}} \tag{2}$$

c_{mes}^{InGaN} and c_{mes}^{GaN} correspond to the values of the out-of-plane lattice parameter c of InGaN and GaN, respectively, as deduced on our samples, since the compressive strain of the 3.5μm thick GaN on sapphire template is around 1%. For InN, we take the unstrained value of the out-of-plane lattice parameter (c_0^{InN}) which is known accurately (within 0.1%) in the literature [19], and equal to 5.705nm. For fully strained layers on GaN template substrates, the out-of-plane and in-plane lattice parameters are related [20] by:

$$\frac{c_{mes}^{InGaN} - c_0^{InGaN}}{c_0^{InGaN}} = -\frac{2 \times \nu}{1 - \nu} \cdot \frac{a_{mes}^{InGaN} - a_0^{InGaN}}{a_0^{InGaN}} \tag{3}$$

where c_{mes}^{InGaN} and a_{mes}^{InGaN} are the experimental out-of-plane and in-plane lattice constants while c_0^{InGaN} and a_0^{InGaN} are the corresponding bulk lattice parameters. ν is Poisson's coefficient which can be interpolated between the values of ν of the two binary end-points. A summary of published data is given in [19], Moram et al. The indium content in fully strained InGaN can thus be calculated according to Eq. (4):

$$x = \frac{1 - \nu}{1 + \nu} \times \frac{c_{mes}^{InGaN} - c_{mes}^{GaN}}{c_0^{InN} - c_{mes}^{GaN}} \tag{4}$$

The luminescence properties of InGaN structures are investigated by both room-temperature (RT) CL and PL measurements. Experimental conditions are given in [21, 22], El Gmili et al. Using a relative least square method, the composition dependences of the emission bandgap energy as deduced from CL measurements are fitted by the standard quadratic Eq. (1).

The estimated value of the error in the determination of the bandgap energy is less than or equal to ±1%. This error arises from the determination of the peak wavelength of the luminescence band. It takes into account the accuracy of both the experimental setup and luminescence band mathematical fit. The error in the determination of the indium composition, as deduced from Eqs. (2) and (4), is estimated to be less than or equal to ±3% for both fully relaxed and strained InGaN layers. These errors are calculated by taking into account (i) the error in the determination, from XRD measurements, of the interplanar spacing d$_{00l}$ of InGaN and GaN

layers which can be calculated using the Braggs law differentiation [19]:

$$\frac{\Delta d_{hkl}}{d_{hkl}} \sim \cot(\Delta\theta_{hkl}) \times \Delta\theta \tag{5}$$

where θ_{hkl} is the Bragg angle, and $\Delta\theta$ the step size in θ ; (ii) the uncertainty in the knowledge of the literature values of both strain-free out-of-plane lattice constant of InN and Poissons coefficient. This estimation leads to indium composition errors equal to $\pm1\%$ and $\pm3\%$ for fully relaxed and strained InGaN layers, respectively. Due to the uncertainty in the knowledge of the literature values of Poissons coefficient, the error is found to be larger in the case of the strained layers. However, in the case of the relaxed layers, the rather scattered experimental InGaN diffraction spots yield an increase of the error in the determination of the values of the lattice parameters. Finally, an error of $\pm3\%$ is estimated for both relaxed and strained InGaN layers.

3. Results and discussion

3.1. Sorting of the InGaN samples according to their strain state rate and indium content

XRD spectra of all the samples were analyzed to determine their indium content, thickness, and strain state rate. Their surface morphology has been also characterized using scanning electron microscopy. Figure 1 summarizes this analysis. According to their morphology, the samples can be sorted in three different sets of samples named A, B, and C. The first set (set A) includes samples exhibiting 2D surface morphology and fully strained InGaN layers, while the third set (set C) comprises samples with 3D surface morphology and fully relaxed InGaN layers. In
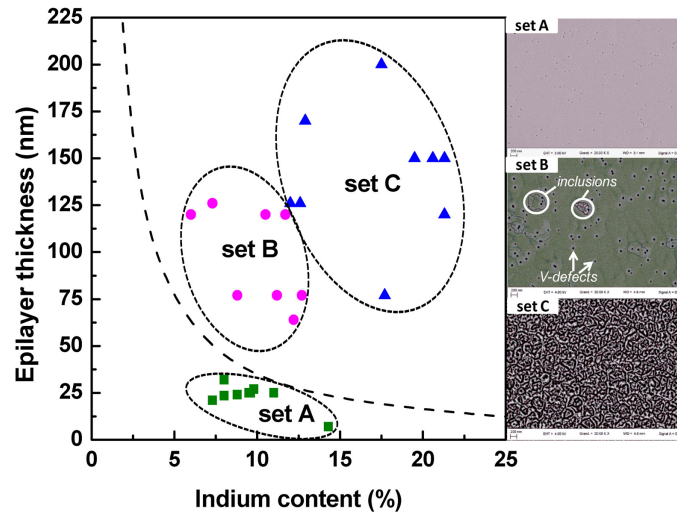

Fig. 1: InGaN surface morphology versus indium composition and epilayer thickness. The theoretical critical layer thickness as deduced from the model of Fisher et al. [23] is also reported (dashed line).

between these two sets, the set B contains samples with 2D surface morphology, in which 3D indium rich inclusions embedded in the 2D InGaN matrix tend to appear [21], and partially relaxed InGaN layers. Such local indium rich domains contribute to the transition from 2D (set A) to 3D (set C) growth mode observed in samples whose thicknesses are larger than the

critical layer thickness. To highlight that point, the critical layer thickness for plastic relaxation computed from the model reported by Fischer et al. [23] is also reported (dashed line) in Fig. 1. According to that model, the critical layer thickness h_c is:

$$\frac{h_c}{\ln \frac{h_c}{B}} = \frac{B \times \cos \lambda}{0.0836 \times x} \times \left(1 + \frac{1 - \frac{\nu}{4}}{4\pi \times \cos^2 \lambda \times (1 + \nu)}\right) \tag{6}$$

where B is Burger's vector magnitude, λ the angle between the Burger's vector and the interface, x the Ga content of the $In_{1-x}Ga_xN$ layer, and ν is Poisson's coefficient as discussed above. The values of Burger's vector used to obtain the curve plotted in Fig. 1, are taken from the literature [24] and are equal to 0.324 nm and 0 degrees for the magnitude and the angle respectively.

To support our previous analysis, typical (11.4) RSMs and (00.2) ω-2θ scans of samples from set A and C are presented in Fig. 2. Peaks related to fully strained (R=0%) and relaxed (R=100%) films with different indium compositions should lie on the vertical and oblique dashed-line, respectively. For clarity, the strained and fully relaxed diffraction spots are named InGaN#1 and InGaN#2, respectively. In Fig. 2(a), the InGaN layer of set A is shown to be fully strained on GaN, as an InGaN diffraction spot lies on the vertical line corresponding to pseudo-morphic InGaN on a GaN template substrate. The indium composition deduced from the (114) RSM and the (004) scan is equal to 10.6%. In addition, the (00.2) XRD ω-2θ scan revealed several diffraction satellites which fit well with 25nm InGaN layer thickness (Fig. 2(b)). For
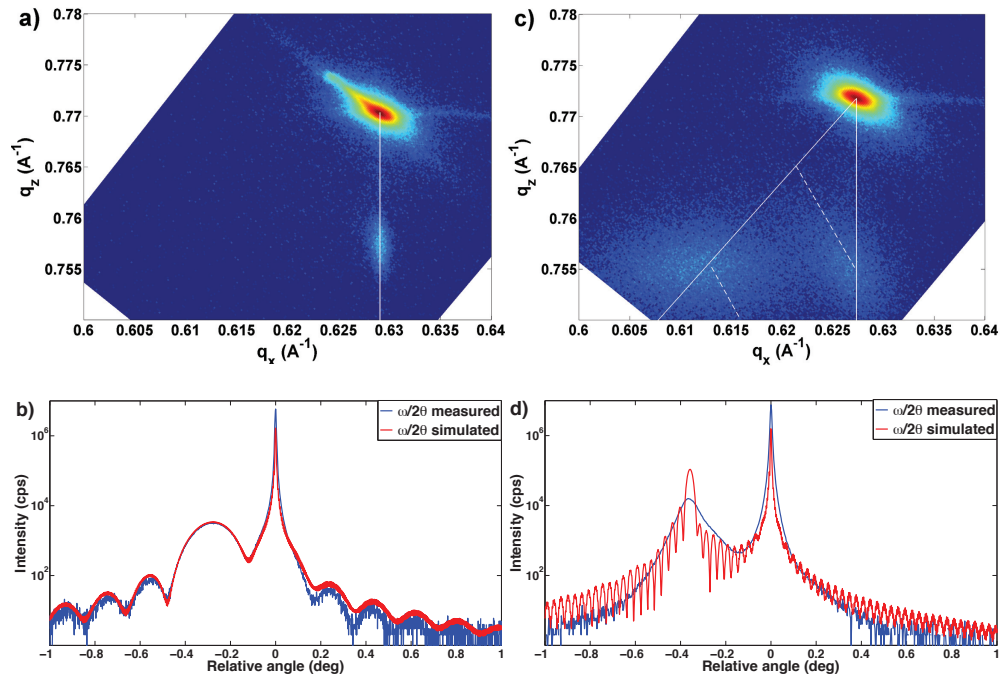

Fig. 2: Examples of typical (114) RSM and $\omega - 2\theta$ XRD scans obtained in the case of (a-b) a sample from set A (2D morphology and fully strained InGaN layers) and (c-d) a sample from set C (3D morphology and fully relaxed InGaN layers), respectively.

thick layers (set C), the asymmetric RSM presents two InGaN diffraction spots, as shown in

Fig. 2(c). As the strain of the film changes at a fixed composition, the peak should move on iso-composition lines (dashed lines) which have been calculated according to the model proposed in [25], Peireira et al. For InGaN#1, the in-plane peak position occurs very close to the value of the GaN template peak (ΔQ_x=-0.0005Å^{-1}) indicating that the film is almost fully strained on the substrate. Furthermore, the position of the second InGaN broad diffraction spot corresponding to a fully relaxed layer indicates higher indium content for InGaN#2 than for InGaN#1. In Fig. 2(d), the $(0\,0\,2)$ scan reveals only one InGaN large diffraction peak with no Pendellösung fringes which is consistent with the 3D surface morphology of samples from set C. The InGaN peak corresponds to a 13.8% indium content partially relaxed (around 6%) InGaN sublayer while indium composition is calculated to be equal to 21.3% for the fully relaxed sublayer (InGaN#2). A structure consisting on a InGaN#2 (R=100%, 120nm) / InGaN#1 (R=6%, 30nm) / GaN template provides a good fit to experimental results, as shown in Fig. 2(d). Since the aim of this paper is the determination of the bandgap bowing parameter in both fully strained and relaxed layers, only results obtained from samples of set A and set C will be considered in the following. Nevertheless, Fig. 3 summarizes RSMs results, showing strain state for all twenty six samples studied in this work.
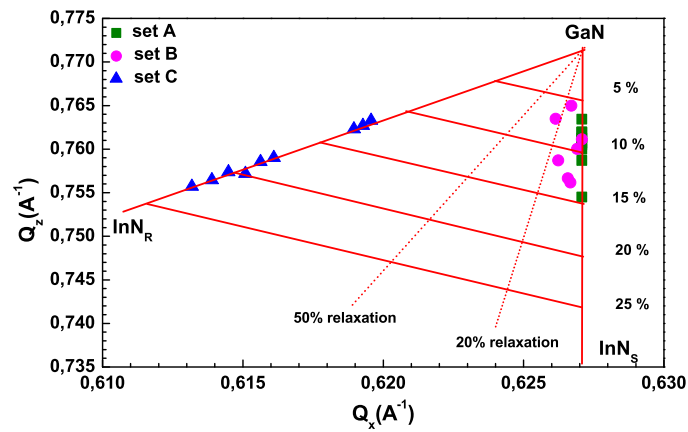

Fig. 3: Summary of RSMs results, showing strain state (for samples of set C only the relaxed sublayer is reported) for all twenty six samples studied in this work.

3.2. *Determination of the bandgap emission energy*

RT depth-resolved CL measurements were performed for electron beam energy varying from 3 to 17keV. For clarity, only the most representative spectra are presented in Fig. 4. Monte-Carlo simulation allows calculation of the overlap shape of the energy loss rate as a function of the layer depth. For an increase of the electron beam energy, the region of maximum loss moves progressively from the near surface to the interface region. As the electron beam energy varies from 3keV to 5keV (12keV), such regions correspond to calculated sample depths of maximum energy loss of 23nm and 46nm (155nm), respectively. Strained films (samples from set A) show two peaks located at around 366nm and 410nm as well as large bands (GaN and InGaN defects transitions [26,27]) whatever the electron beam energy (Fig. 4a). The peaks are attributed to the GaN template substrate and InGaN layer, respectively. The variation in intensity of both peaks with electron beam energy is in agreement with Monte-Carlo simulations. For the samples of set C, CL spectra change drastically with the acceleration voltage, as shown in Fig. 4b. At 3keV, we observe only the InGaN peak at around 510nm and a broad band centered close to 650nm (In-
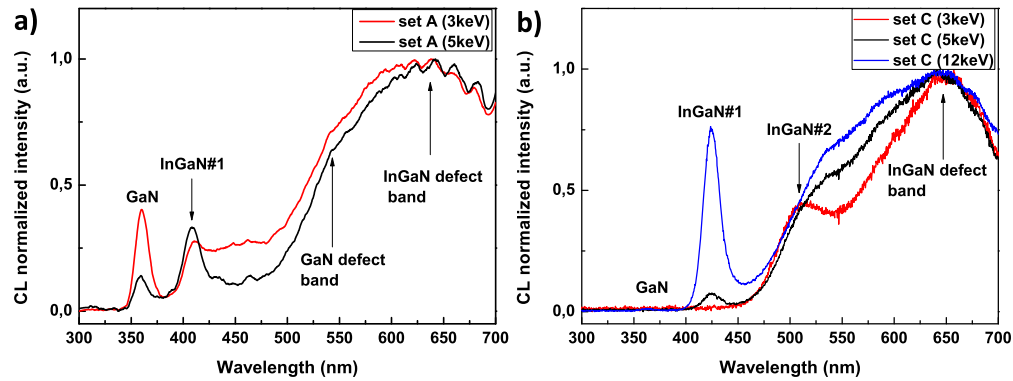
Fig. 4: Typical room temperature CL spectra obtained at different electron beam energy for samples from set A (a) and set C (b).

GaN defect band). For an increase of the electron beam energy to 5keV, a second peak appears at lower wavelength (425nm). The splitting of both InGaN CL peaks can be explained in terms of strain relaxation and/or indium composition fluctuation. However, this value is huge (around 438meV) compared to that calculated for both relaxed and strained peaks positions by Pereira et al. [28] for an indium content of 10% and equal to 150meV. Thus, the splitting observed in Fig. 4b cannot be only explained by strained relaxation but also by an increase on the indium composition in InGaN in agreement with the XRD RSM reported in Fig. 2(c). According to such results as well as to Monte-Carlo simulations, the 425nm and 510nm wavelength peak positions are attributed to InGaN#1 (strained InGaN) and InGaN#2 (relaxed InGaN) sublayers, respectively. This interpretation is also confirmed by a nanometer-scale, quantitative composition mapping of InGaN layers obtained from a combination of scanning transmission electron microscopy and energy dispersive x-ray spectroscopy on some of the samples and conducted in a previous study [29, 30].

3.3. Determination of the bandgap energy bowing parameters

Figures 5a and 5b show the indium content dependencies of the bandgap emission energy as deduced from PL and CL measurements for both fully strained and relaxed InGaN layers, respectively. The value of the bandgap emission energy bowing parameter b can be deduced from these data using a relative least squares method. We have thus conducted such a least squares fit using Eq. (1) and the data of Fig. 5 for both extreme state of strain of the InGaN layers. The GaN bandgap was measured as 3.39eV (RT CL) in agreement with the value reported at 300K by Yam et al. [31] and Islam et al. [8]. That of bulk InN is subject to variations in the literature. We have taken into account values varying between 0.64eV and 0.77eV at 300K [11, 32, 33], and estimated the bandgap bowing parameter b for relaxed layers within this range of values. Furthermore, in the case of strained layers, to calculate the bandgap of pseudomorphic InN on GaN template we have used the input equation and deformation potentials of references [34,35]. The effect of the strain leads to a theoretical increase of the InN bandgap of 0.1eV. For strained layers, the value of b can thus be fitted for InN bandgaps in the range of 0.74eV to 0.87eV. Conducting fits for many values of the InN bandgap shows that the InN bandgap energy dependences of the bowing parameter b can be described by the following linear equations for
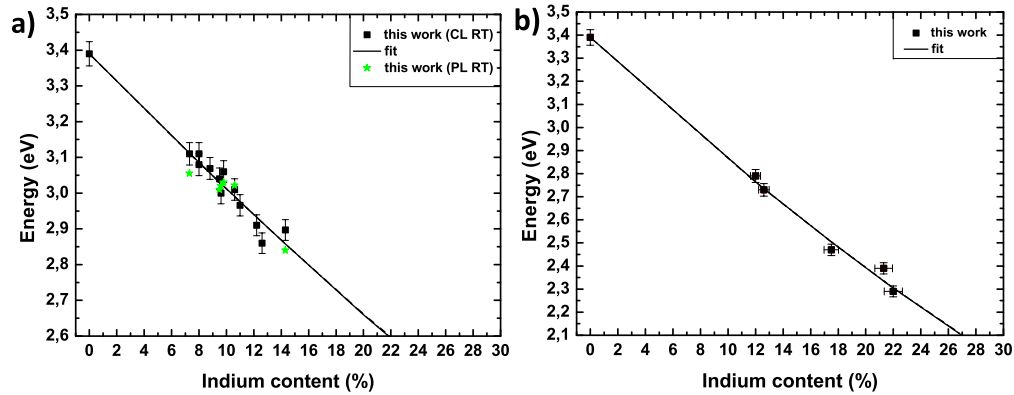
Fig. 5: Low In content dependence of the bandgap emission energy in fully strained (a) and relaxed (b) InGaN layers. The solid lines represent the best relative least squares method fit according to Eq. (1). For an InN bandgap energy of 0.7eV, the values of the bowing parameter are equal to 1.32 ± 0.28eV and 2.87 ± 0.2eV for fully strained and relaxed InGaN layers, respectively.

strained and relaxed layers, respectively:

$$\begin{cases} b^{(strained)} = 1.154 \times E_g^{InN} + 0.396 \\ b^{(relaxed)} = 1.230 \times E_g^{InN} + 2.010 \end{cases} \tag{7}$$

For both states of strain, we have assumed that, if the InGaN bandgap measurement was done again, there would be 95% chance that the new measurements fall within a 3% maximum distance from the initial measurement. In other words, the bandgap measurement is obtained with a 6% precision at a 5% risk. As no precise statistical method can be found in the literature to take into account the errors on both variables within a statistical fit, we also assume an exact measurement of the composition value. In terms of possible errors on the determination of the values of b, they are to be understood differently for each state of strain. We found that, for the relaxed sample, there was more than 70% chance that the quadratic model is able to correctly describe our measurements. Thus, assuming the quadratic model truthfulness, b is found to fall at a maximum distance of 0.2eV from the values given on the figure with 95% chance. For the strained sample, the model truthfulness probability rises to more than 90%, whereas the maximum error on b, with a 5% risk, is 0.28eV. The possible measurement errors on the bandgap that we have taken into this statistical study are slightly higher than those that have been estimated independently above. This is not surprising and not contradictory since we have not taken into account, in the statistical analysis, the possible errors on the composition, which are in fact relatively greater than that on the bandgap. The linear dependence of b with respect to E_g^{InN} (Eq. (7)) allows us to obtain the value of the bandgap bowing parameter from the measured value of the InN bandgap. For instance, a bulk InN bandgap energy of 0.70eV would lead to values of b equal to 2.87 ± 0.2eV and 1.32 ± 0.28eV for relaxed and strained layers, respectively. Table 1 summarizes the values of the bandgap energy bowing parameter b obtained in the frame of this work and compared to values reported by different other authors. To our knowledge, the value of b for strained layers is reported for the first time since the re-evaluation of the InN bandgap. For relaxed samples, our value of b is consistent with the results of Islam et al. [8] and Moret et al. [9] and quite different from the data of Kurouchi et al. [10].

Using the values of the bowing parameter b and Eq. (1), it is possible to extrapolate the indium

Strain state	[In] (%)	E_g^{InN} (eV)	b (eV)	Experimental	Reference
strained	0 - 15	0.74 - 0.87	1.25 - 1.40	CL	This work
relaxed	0 - 25	0.64 - 0.77	2.8 - 2.96	CL	This work
relaxed	0 - 40	-	2.62	PL	[8]
relaxed	61 - 100	0.66	1.8	PL	[10]
relaxed	0 - 100	0.8	2.8	PL (10K)	[9]

Table 1: Room temperature values of the emission bandgap energy bowing parameter b obtained in the frame of this work and compared to values reported by different other authors since the InN bandgap re-evaluation. Note that the data of Moret et al. [9] are obtained at 10K.

content dependence of the bandgap energy of the InGaN alloys to the whole indium content range and for the different InN bandgap values. Figures 6a and 6b show values of the bandgap energy measured within this work and by other authors, as well as their extrapolations for both strained and relaxed InGaN layers. As can be seen, for both strain state of the layers, our results
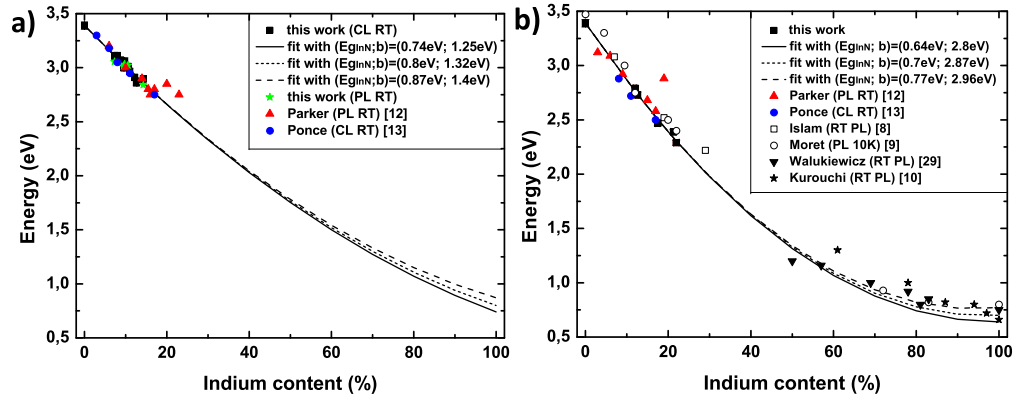

Fig. 6: Extrapolation of the In content dependence of the bandgap energy of InGaN alloys to the whole indium content range according to the different InN bandgap values, for a) strained and b) relaxed layers. Data obtained in this work and by other authors are shown for comparison.

are in good agreement with data of references [8, 12, 13]. Data of Moret et al. [9], which have been obtained for composition close to the two binary endpoints and at low temperature, are slightly larger than our experimental values. Such a difference is consistent with the temperature bandgap variation described by the Varshni's equation. For indium-rich InGaN alloys, the data of [32], Walukiewicz et al., and [10], Kurouchi et al., seem to be in a better agreement with the fits whose InN bandgap energy and bowing parameters values are equal to 0.77eV and 2.96eV, respectively.

3.4. *Indium content mapping of thick InGaN layers*

As an example, we apply the modified Vegard's laws, describing accurately the indium content dependence of the bandgap emission energy in InGaN alloy and for the whole range of indium content, to build 3D mapping of indium content in a thick InGaN layer from bandgap energy

measurement using CL and a corresponding hyperspectral map. For this, using the modified Vegard's laws, the change in the wavelength peak (or energy) position can be converted into composition variation for a given state of strain. This is applied to a 130nm thick InGaN layer from the set of samples C. XRD measurements analysis on this sample indicate a structure consisting in a 120nm thick, almost fully relaxed, InGaN#2 layer with 25% of In content, on a 30nm thick, almost fully strained (0.7% of relaxation), InGaN#1 layer with 14.1% of In content. The spatial variation of the luminescence was recorded for different electron beam energy through 400 points over a top sample surface of $5 \times 5\mu m^2$. The corresponding CL hyperspectral mappings obtained at 3keV and 7keV which correspond to the maximum of CL intensity expected for InGaN#2 and InGaN#1 sublayers are presented in Fig. 7a and Fig. 7b, respectively. The plot of the corresponding compositional variation calculated by taking into account the strain state (deduced from XRD RSM measurements) of each sublayer and according to the different Vegard's laws and thus values of the bandgap energy bowing parameter b are shown in Fig. 7c and Fig. 7d. The two sublayers exhibit rather large inhomogeneities. For the near-
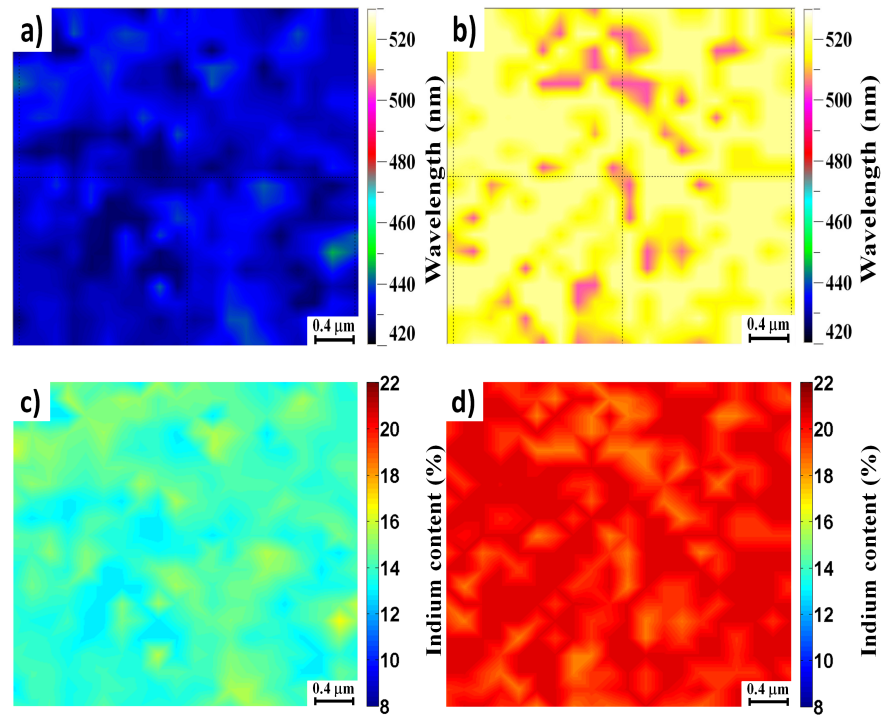

Fig. 7: CL hyperspectral maps (a-b) and corresponding indium content maps (c-d) of a 130nm thick InGaN layer from the set of samples C obtained for electron beam energy of 3keV (b-d, InGaN#2 sublayer) and 7keV (a-c, InGaN#1 sublayer).

surface sublayer (InGaN#2) the average indium content is roughly equal to 21% and varies down to 18% at some places. Such compositional inhomogeneity is consistent with the broad InGaN#2 diffraction spot observed on the XRD RSM (not shown here). Near the InGaN/GaN interface, the InGaN#1 sublayer should be more homogeneous. It is not fully the case. This can be explained by the larger electron beam energy required to reach the InGaN#1 sublayer, and thus larger interaction region including the InGaN#2 sublayer. Some indium content fluctuations that appear in Fig. 7b can thus be attributed to the latter. Nevertheless, an average indium

content of 14.5% with some variations down to 13% can be seen in the InGaN#1 sublayer.

4. Conclusion

We have determined the bandgap energy bowing parameter of both strained and relaxed In-GaN layers. The indium content bandgap energy dependence was fitted using a least square method leading to a range of values of the bowing parameter according to the value of the InN bandgap energy. Our results are demonstrated to be significant for CL measurements and especially to map the spatial compositional variation of a given sample with different state of strain. This work also provides interesting tools for the analysis and characterization of InGaN-based nanostructures and heterostructures.

Acknowledgment